Cutting floating single-walled carbon nanotubes with a 'CO$_2$ blade'

Ying Tian [a, b], Nan Wei [b], Patrik Laiho [b], Saeed Ahmad [b], Yann Magnin [c], Yongping Liao [b], Christophe Bichara [d], Hua Jiang [b, *], Esko I. Kauppinen [b, **]

[a] Department of Physics, Dalian Maritime University, Dalian, Liaoning, 116026, China
[b] Department of Applied Physics, Aalto University School of Science, Puumiehenkuja 2, 00076, Aalto, Finland
[c] MultiScale Material Science for Energy and Environment, Massachusetts Institute of Technology-CNRS Joint Laboratory at Massachusetts Institute of Technology, Cambridge, MA, 02139, USA
[d] Aix-Marseille University and CNRS, CINaM UMR 7325, 13288, Marseille, France

ABSTRACT

Uniform ultra-short (<100 nm) single-walled carbon nanotubes (SWCNTs) with properties of rich chemistry, high dispersity and easy manipulation, are of great importance for constructing novel nano-structures and highly integrated miniature devices. Herein, we report a recent breakthrough in cutting long SWCNTs into uniform ultra-short segments in gas-phase using CO$_2$ as a 'blade.' SWCNTs synthesized by an aerosol reactor are directly introduced into a second reactor for gaseous cutting. The quality and the number concentration of shortened SWCNTs are enhanced after the gas-phase cutting process. Moreover, the growth and cutting of SWCNTs are accomplished in a continuous gas-phase process, thus allows direct dry deposition of ultra-short SWCNTs as individual macromolecules or thin films onto various substrates for multiple applications.

© 2018 Elsevier Ltd. All rights reserved.

1. Introduction

Single-walled carbon nanotubes (SWCNTs) which possess outstanding mechanical, optical and electrical properties, are promising building blocks for constructing advanced nanoscale structures and devices [1,2]. Typically, as-synthesized CNTs are of a few micrometer long and they are easily bundled and entangled with each other. This entangled nature and chemical inertness of long CNTs make it difficult to integrate them into other materials or nano-devices [3]. The CNT entanglement decreases dramatically with their lengths reduction. Good solubility and homogeneous dispersion of CNTs in aqueous solution [6], polymer [7,8] and metal matrix composites [9,10] have been achieved after shortening the CNTs length down to a few hundreds of nanometers, thus realize optimal mechanical and optical performance. Furthermore, shortened-SWCNTs have rich chemistry due to the fact that their ends are either open or curvedly closed, which is critical for func-tionalization with chemical or biological molecules [5]. In partic-ular, ultra-short SWCNTs (less than 100 nm) with uniform length

distribution are of great importance in constructing novel nano-structures and miniature devices in wide applications such as drug delivery [11,12], targeting [13], molecule sensor and probes [14], plasmonic resonators [15] and scaled transistors [16].

In order to achieve SWCNTs with preferably short lengths, one practice is to cut long CNTs short [4,5]. Many efforts have been made to develop efficient techniques to cut CNTs. Among those reported work, one popular way is to use chemical method with strong oxidants, such as concentrated sulphuric and nitric acid [5], piranha solution [4], Fe$_2$O$_3$ [6] and ozone [17]. However, the strong oxidations usually cause loss of carbon materials and introduce a number of defects during the aggressive oxidation processes. The resultant shortened CNTs have lengths in a wide range of 50–700 nm [3,4]. An improved chemical method is based on the fluorination process followed by pyrolysis at 1000 °C in Argon [18]. This method is considered an efficient cutting method with an overall carbon yield of 70–80% and can cut SWCNTs with length between 20 and 300 nm. Other common strategies of shortening CNTs are ball-milling [19,20], cryogenic crushing [21], ultrasonic treatments [22], as well as electron-beam [23,24] and ion etching [25]. However, besides the issues of material loss and quality de-grades, these processes can hardly control the length uniformity, or costly equipment is needed. Up to date, all cutting procedures have been performed in liquid or solid phases. And in many cases, liquid

* Corresponding author.
** Corresponding author.
E-mail address: hua.jiang@aalto.fi (H. Jiang).

or solid additives (e.g., $FeSO_4 \cdot 7H_2O$ [6], polymers [17], ammonium persulfate [26], cobalt acetylacetonate [27], and diamond particles [22]) are needed for the cutting or for the improvement of cutting efficiency. These additives contaminate the resultant CNTs and lead to extra efforts to remove them afterwards. Therefore, there exist a number of issues in the current techniques that hold back the promising applications of short-CNTs.

Herein, we report an approach of cutting floating SWCNTs in gas phase. The resultant SWCNTs uniquely preserve high quality and uniform ultra-short length (<100 nm). In particular, the growth as well as the cutting process of the nanotubes are accomplished continuously in gas phase, which allows direct and dry deposition of the cut-SWCNTs as individuals or as the thin film of desired thickness onto the substrates. Such a simple manipulation of ultra-short nanotubes offers a reliable methodology for building novel miniature devices and enables a number of promising applications of the ultra-short SWCNTs in future molecular science.

2. Experimental

2.1. SWCNT synthesis and cutting process

2.1.1. Aerosol synthesis reactor (reactor I)

SWCNTs were grown in an aerosol reactor with spark-generated iron (Fe) particles as catalysts and carbon monoxide (CO) as carbon source [28]. Fe catalyst nanoparticles were generated inside the spark generator consisting of two rode-shaped Fe electrodes that were discharged through a capacitor (C = 47 nF) using a high-voltage of 3 kV. A high velocity of nitrogen (N_2, 40 lpm) was used to flush the formed Fe particles between the two electrodes and further carry them (limited to 210 cm^3min^{-1}, the rest N_2 goes to exhaust) into the aerosol reactor at 750 °C. The hydrogen (H_2, 40 cm^3min^{-1}) and CO (250 cm^3min^{-1}) were introduced into the aerosol reactor for the growth of SWCNTs. The SWCNTs grown in the aerosol growth reactor were either directly collected for characterizations or further introduced into the aerosol cut reactor.

2.1.2. Aerosol cut reactor (reactor II)

The floating SWCNTs produced from aerosol synthesis reactor were introduced into the second aerosol reactor (*Reactor II*) for cutting process using CO_2 as an agent. A total gas flow of 500 cm^3min^{-1} carrying SWCNTs from *Reactor I* was introduced into the *Reactor II* with temperature set at 520 °C. The flow of CO_2 introduced into *Reactor II* ranges from 34 to 374 cm^3min^{-1} giving CO_2 volumetric concentration from 6 to 43%.

The SWCNTs from either *Reactor I* or *Reactor II* can be directly collected on TEM grids or nitrocellulose membrane filters (Millipore Corp., USA). SWCNT thin films were deposited on mica or patterned substrates using thermophoretic precipitator (TP) [29].

2.2. Characterizations

2.2.1. Real-time measurements

Real-time number size distributions (NSDs) of catalyst particles and SWCNTs were detected by using a scanning mobility particle sizer with Faraday Cup electrometer (SMPS + E, GRIMM Aerosol Technic GmbH, Germany). We measured the real-time NSDs of Fe catalyst particles at the inlet of *Reactor I*, and SWCNTs at the outlets of *Reactor I* and *Reactor II*, respectively. By controlling number concentration (NC) of catalyst particles, we maintained the SWCNTs with NC about 2×10^5 cm^{-3} at outlet of *Reactor I*, which effectively eliminating the nanotube collisions during growth and obtaining up to 80% individual SWCNTs.

2.2.2. Morphology characterizations

The morphology and length distributions of SWCNTs were characterized using high-resolution transmission electron microscopy (HR-TEM) and atomic force microscopy (AFM). For TEM analysis, as-grown SWCNTs collected on TEM grids were measured with a double aberration-corrected microscope (JEOL-2200FS, JEOL Ltd., Japan). AFM (Dimension 5000, Veeco Instruments, Inc., USA) observations were performed at optimized settings [22] on SWCNTs which was thermophoretically deposited onto mica substrates.

2.2.3. Optical characterizations

The purity and diameter distributions of SWCNTs were characterized by measuring absorption and Raman spectra. The SWCNT thin films were transferred from membrane filter onto transparent quartz substrate (material: HQS300, Heraeus) using a press-transfer technique for the optical absorption measurements (Perkin-Elmer Lambda 950 UV-Vis-NIR spectrometer). Raman spectra were performed on a Labram-HR 800 (Horiba Jobin-Yvon) Raman spectrometer using laser wavelengths of 514 and 633 nm. Raman spectra were averaged based on the measurements of three different points of each thin film samples. An 1800 mm^{-1} grating was utilized for a high spectral resolution of 1 cm^{-1}.

3. Results and discussion

Fig. 1a shows a schematic of continuous gas phase growth and the subsequent cutting process of SWCNTs in two sequential aerosol reactors. The SWCNTs were grown in the aerosol reactor (*Reactor I*) at 750 °C, fed with a flow of carbon monoxide (CO, 250 cm^3min^{-1}), hydrogen (H_2, 40 cm^3min^{-1}), and nitrogen (N_2, 210 cm^3min^{-1}) carrying iron (Fe) catalyst particles that were formed by a spark discharge generator [28]. The floating as-grown SWCNTs with a total gas flow of 500 cm^3min^{-1} were then introduced into the second aerosol reactor (*Reactor II*) for the gaseous cutting process. To preserve the quality, as-grown SWCNTs were cut by a weak oxidizing agent of carbon dioxide (CO_2) at a relatively low temperature of 520 °C. The CO_2 flow from 34 to 374 cm^3min^{-1} was introduced into the *Reactor II*, which corresponds to the volumetric concentration from 6 to 43%.

Atomic force microscopy (AFM) was used to measure the lengths of carbon nanotubes. For AFM observations, the floating SWCNTs were directly deposited onto the mica substrates from the outlets of the two aerosol reactors, respectively, using a thermophoretic precipitator (TP) [29]. As shown in Fig. 2, the mean length of as-synthesized SWCNTs is about 1.2 μm. After the cutting procedure at CO_2% of 6%, the lengths of SWCNTs are efficiently cut down to ≈78 nm with a narrow length distribution. It is noted that nearly 76% nanotubes have lengths in the range from 40 to 100 nm. Remarkably, as the CO_2 concentration increases up to 43%, the lengths of SWCNTs are further shortened. The fraction of nanotube lengths less than 40 nm significantly increases from 4% up to 21%, resulting in nanotubes with a mean length of ≈64 nm. Interestingly, we observed an interesting phenomenon in AFM images that many cut-SWCNTs show bright dot-like contrast in their ends. Such features are also observed, then further studied with high-resolution TEM (HR-TEM) measurements that will be discussed later.

The cutting process has increased the number concentration (NC) of SWCNTs. We measured the real-time NC distributions of SWCNTs at the outlets of *Reactor I* and *II*, respectively, using a scanning mobility particle sizer with Faraday Cup electrometer (SMPS + E). It has been reported that the NC of Fe catalyst particles between 10^5 and 10^6 cm^{-3} is desired to both avoid significant deposits of inactive catalyst aggregates on the nanotubes and prevent their bundling [28]. By controlling the NC of Fe catalyst particles at
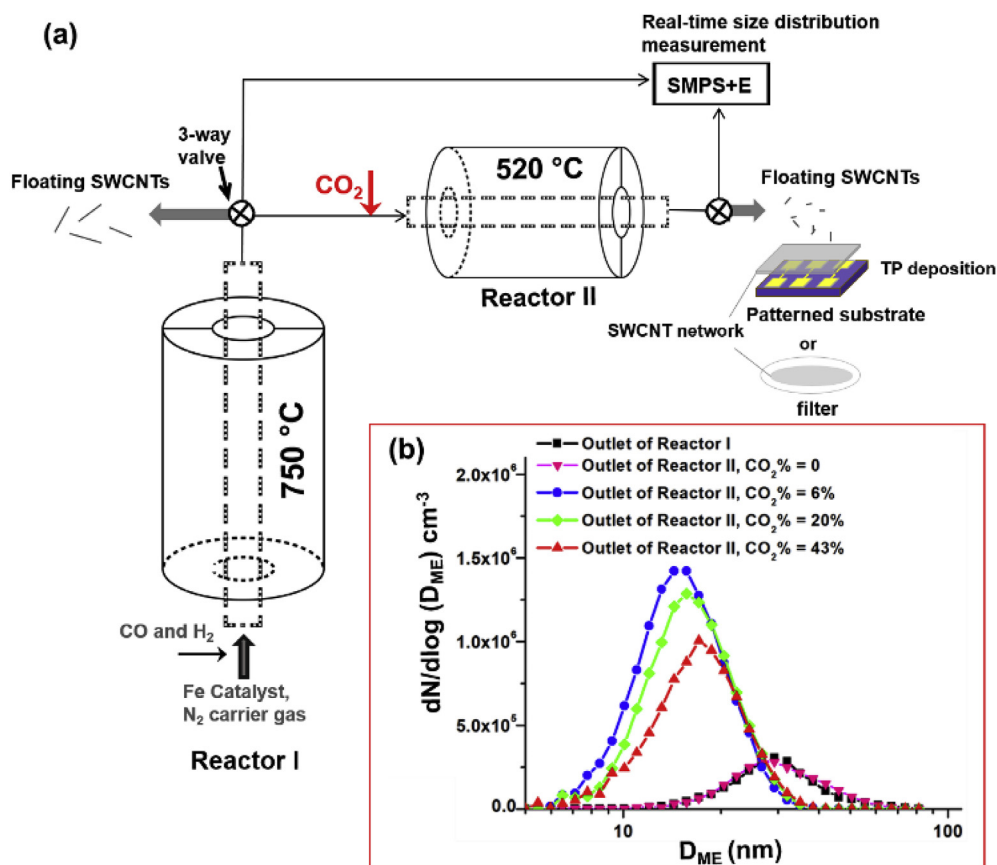
Fig. 1. (a) Schematic representation of the experimental setups of SWCNTs growth in an aerosol reactor (*Reactor I*) and the cutting process of SWCNTs in a second aerosol reactor (*Reactor II*). (b) The real-time number size distributions of as-synthesized SWCNTs measured at outlet of *Reactor I* (black curve), and SWCNTs measured at outlet of *Reactor II* at introduced CO_2% from 0 to 43%. (A colour version of this figure can be viewed online.)

~10^5 cm^{-3}, we maintain SWCNTs with a NC about 2×10^5 cm^{-3}, as shown in Fig. 1b (black curve). Such a low NC of SWCNTs can effectively eliminate the nanotube bundling during growth, thus produces up to 80% individual SWCNTs [28]. By directly introducing the as-grown floating SWCNTs from *Reactor I* into the *Reactor II*, the NC measured at outlet of *Reactor II* remains the same when no CO_2 is introduced (pink curve in Fig. 1b). This implies that the cutting does not occur in *Reactor II* without adding CO_2. This result agrees with the scanning electron microscope (SEM) measurement (Fig. S1), which shows similar nanotube lengths of $\approx 1.0\,\mu m$ to that of the SWCNTs collected from *Reactor I*. However, when small amount of CO_2 (6% by concentration) is added, we observed that the NC of SWCNTs has significantly increased by more than 2-fold from 2×10^5 to 5×10^5 cm^{-3} (blue curve in Fig. 1b). Meanwhile, the electrical mobility geometric mean diameter (D_{ME}) decreases from 30 to 15 nm. The D_{ME} presents a relationship between the nanotube diameters (d_t) and their lengths (l) via $D_{ME} \propto d_t \sqrt[3]{l/d_t}$ [30]. Therefore, such dramatic decrease in D_{ME} indicates the effective shortening of SWCNT length, since the d_t distributions are rather the same for the as-synthesized and the shortened-SWCNTs at low CO_2% of 6%. As shown in the absorption spectra (AS) in Fig. 3a, these two samples present the same absorption features.

By further increasing the CO_2 concentration, the NC of cut-SWCNTs decreases slightly, while the D_{ME} of SWCNTs increases gradually. The typical NSDs of cut-SWCNTs at CO_2 concentrations of 0, 6%, 20% and 43% are plotted in Fig. 1b. Such a decrease in NC and increase of D_{ME} may result from the etching effect of relative smaller diameter nanotubes with the very high CO_2 concentration [31]. This result agrees with the AS measurements which show an

obvious intensity decrease of the absorption peak at ~1190 nm. This peak represents the first transition energy of semiconducting nanotubes with relatively small d_t.

It is worth to note that, in contrast to previous reports where the quality of cut-SWCNTs has deteriorated due to the defects and tube damages induced by the strong cutting treatments [2], [7], [10], [13,20], our mild gas-phase cutting approach has effectively preserved the quality of cut-SWCNTs. Fig. 3b shows Raman spectra of both the as-grown and the cut-SWCNT samples at excitation of 514 nm laser, exhibiting the typical Raman features\ from SWCNTs that are radial breathing modes (RBMs), tangential (G) and disorder-induced (D) bands [32]. After normalization of G bands, we observe an obvious drop in the D band intensity after the cutting procedures. Such intensity decrease in the D band indicates that the gas-phase cutting by CO_2 at relative low temperature of 520 °C introduces little defects or disordered structures to the cut-SWCNTs. On the contrary, the fact that CO_2 can etch away the amorphous carbon from the surfaces of nanotubes would further improve the quality of the shortened SWCNTs [31,33]. Since the diameter ranges of all three samples are similar, their RBMs all appears at the same range of 180–280 cm^{-1}. Similar results were observed in Raman spectra measured with 633 nm laser (Fig. S2).

To understand the mechanisms of using CO_2 to cut SWCNTs, we performed electron microscopy studies on both as-synthesized SWCNTs and cut-SWCNTs (CO_2 at 43%). Fig. 4a shows typical HR-TEM images of as-synthesized SWCNTs, which contain both individual (the inset) and bundled nanotubes. It is noted that a number of fullerene-like structures are observed attaching to the sidewalls of the as-grown nanotubes. Especially, the fullerene structures

(a) as-synthesized SWCNTs

(b) cut-SWCNTs at CO_2% of 6%

(c) cut-SWCNTs at CO_2% of 43%
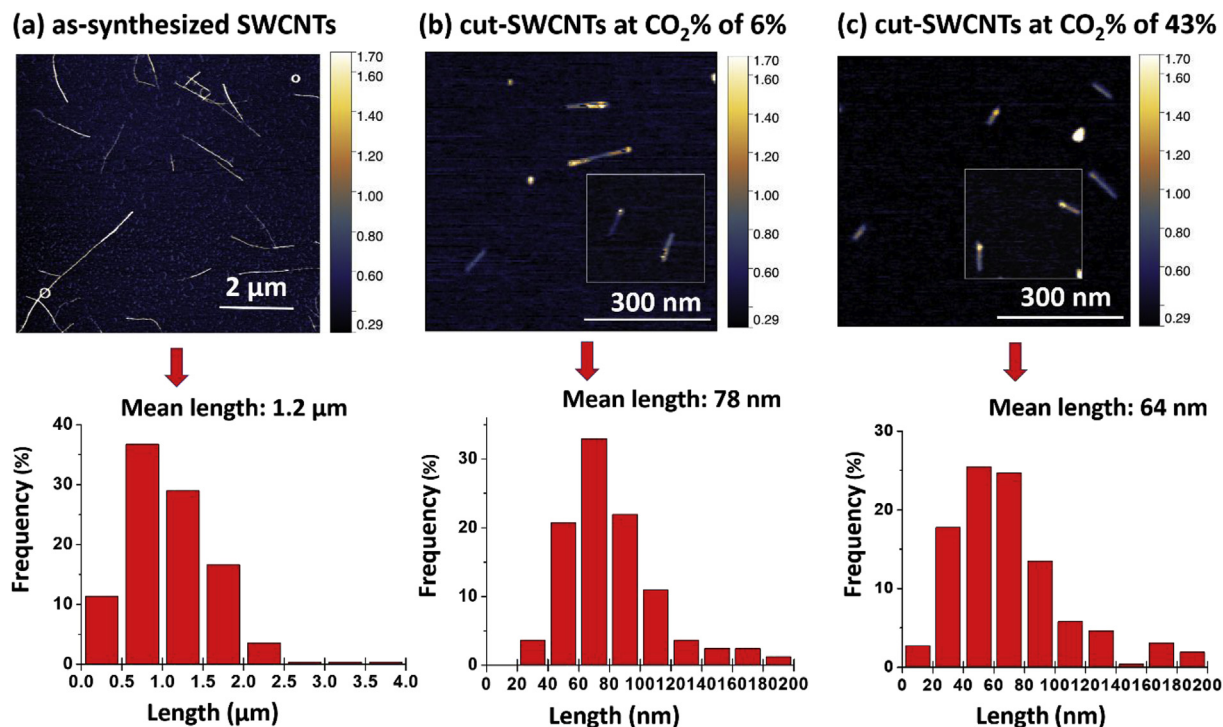
Fig. 2. AFM images and length distributions of (a) as-synthesized SWCNTs and cut-SWCNTs at CO_2 concentrations of (b) 6% and (c) 43%, respectively. The histograms show the mean lengths of the three samples are 1.2 μm, 78 nm and 64 nm, respectively, calculated from the statistics of 282, 180, and 264 SWCNTs. It is observed that some cut-SWCNTs show bright dot-like contrast at the ends. (A colour version of this figure can be viewed online.)

inevitably introduce defects onto the nanotube sidewalls. These existing defective sites are naturally reactive and tend to serve as initiative site for the cutting. Fig. 4b displays a typical TEM image of the cut-SWCNTs collected on a thin carbon supporting film. Apparently short-SWCNTs with uniform lengths are present. Similar to the AFM observation (Fig. 2b and c), TEM images of cut-SWCNTs show also small dot-like features at their ends, as indicated by the red circles (Fig. 4d). Further high-resolution TEM observations of such dark dots (Fig. 4c and d), as indicated by the red arrow in TEM images, clearly show that the dark particles at end of the cut-SWCNTs are tangled carbon coils. These curved carbon coils may provide an easy facility to functionalize the nanotube structure with chemical and biological molecules, which are essential to direct assemble ultra-short SWCNTs into molecular devices or to construct novel functional nanostructures.

CO_2 is believed to play critical etching roles in the efficient cutting of SWCNTs in *Reactor II*. In previous reports [31,33,35], it has been reported that introduction of a certain amount of CO_2 into the growth aerosol rectors (ferrocene-CO-based) can effectively improve the nanotube quality and tune the diameters of SWCNTs. Interestingly, in the current experiment the improvements of the quality of shortened SWCNTs are also observed. Obviously, CO_2 plays a role in etching against amorphous carbon coated on the nanotubes due to the inverse Bouduard reaction [33], thereby enhancing the quality of SWCNTs. Such etching effect by CO_2 was also believed to significantly affect the nucleation and growth of SWCNTs, resulting in the nanotube diameter tuning [33,35]. The above studies shed lights on the fact that CO_2 can selectively etch away more reactive carbon (C) atoms by reversing the Bouduard reaction: $CO_{(g)} + CO_{(g)} \Leftrightarrow C_{(s)} + CO_{2(s)}$, $\Delta H = -169\ kJ/mol$. This etching role by CO_2 is believed to be the key factor to cut as-grown SWCNTs in *Reactor II* after the nanotube growth. In particular, we observed the structure defects introduced by fullerene-like

structures on the sidewalls of as-grown SWCNTs (Fig. 4a). These existing defective C atoms are much more reactive than those in the perfect graphene networks, thereby can be prior attacked by the etching agent of CO_2.

To further gain insight into the cutting process by CO_2, we performed Grand Canonical Monte Carlo (GCMC) calculation on a system where a C_{60} fullerene is attached to a (14,0) tube. The chemical reaction that involves CO_2 to etch against C atoms through a reverse Boudouard reaction, is translated in the GCMC algorithm into a change of chemical potential. The detailed simulation description and snapshots of atomic configurations (Fig. S3) are provided in the supporting information. From the simulation video (in supporting information), we clearly see that the etching of C atoms initiates from the sites between the fullerene cap and the tube, where C—C bonds are weaker than those in a perfect fullerene molecule or a nanotube. In addition, the etching of C atoms and the subsequent formation of vacancies with increasing size take place in the tube, while the fullerene cap remains unaffected. As required in Monte Carlo simulations that drag the system towards thermodynamic equilibrium, long atomic relaxations are performed after each accepted C removal, as well as attempts to incorporate C atoms in the structure. Because of this, we see that the open wounds in the tube tend to heal, yet not completely. These calculations demonstrate that carbon atoms etching starts from the weak links of the structures, which are supposed to be more chemically reactive.

Supplementary video related to this article can be found at https://doi.org/10.1016/j.carbon.2018.11.035

4. Conclusion

In summary, we have developed a strategy of cutting long SWCNTs into uniform ultra-short segments in a continuous gas-phase process by using CO_2 as oxidant. This gaseous cutting
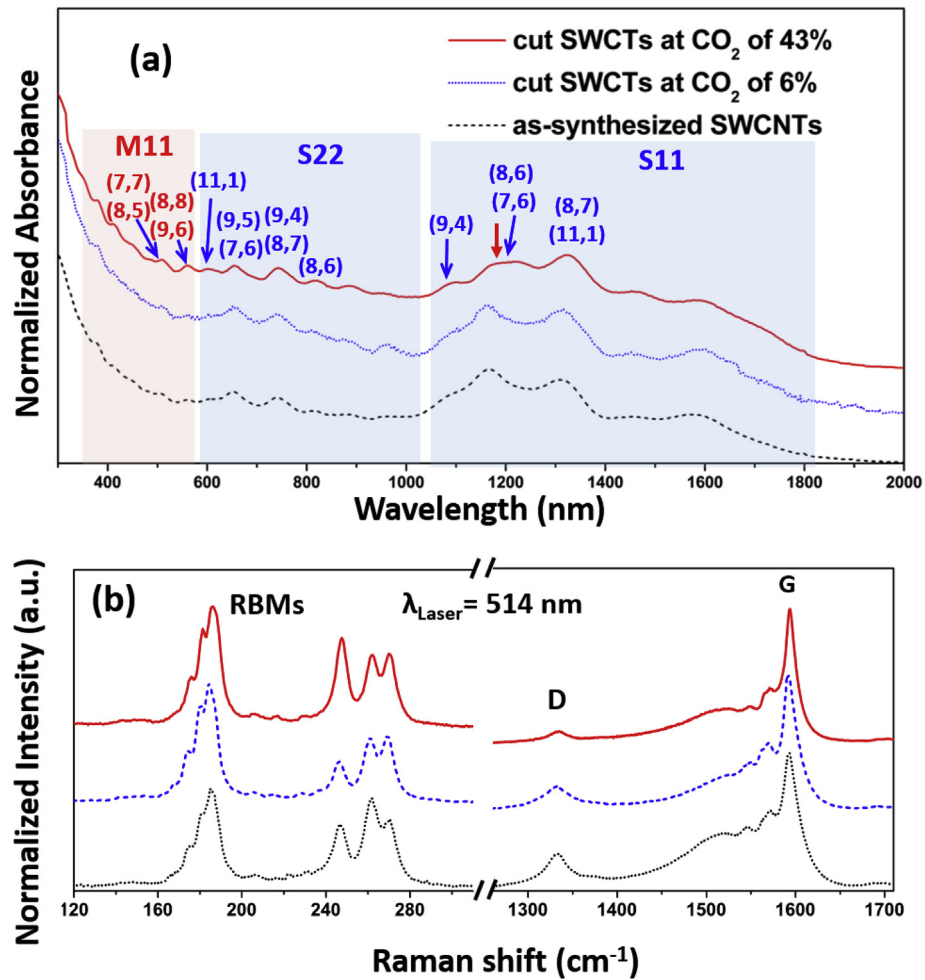
Fig. 3. Absorption (a) and Raman (b) spectra of as-synthesized SWCNTs collected from *Reactor I* (black dots), cut-SWCNTs deposited from *Reactor II* at CO_2 concentration of 6% (blue dashes) and 43% (red solid lines), respectively, at $\lambda_{Laser} = 514$ nm. The assignments of chirality are indicated in the AS spectra. The RBMs and G,D bands of SWCNTs are marked in the figure. (A colour version of this figure can be viewed online.)
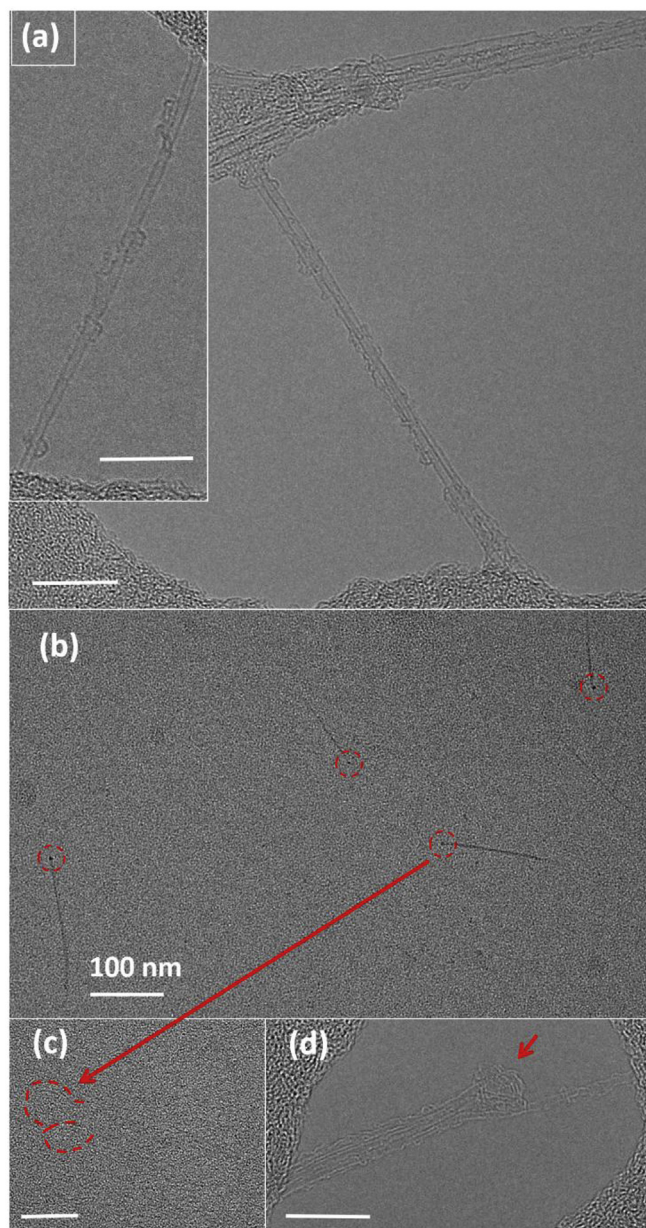
Fig. 4. TEM images of (a) as-synthesized SWCNT, (b) cut-SWCNTs, (c) and (d) HRTEM images of the end of short tubes. The scale bar is 10 nm or otherwise indicated in the images. (A colour version of this figure can be viewed online.)

approach exhibits a remarkable advantage over conventional cutting process in enhancing quality of the cut-SWCNTs. Moreover, owing to the unique continuous gas-phase process, the uniform ultra-short SWCNTs can be directly deposited from gas-phase onto various substrates at ambient condition for multiple applications.

Acknowledgment

Appendix A. Supplementary data

Supplementary data to this article can be found online at https://doi.org/10.1016/j.carbon.2018.11.035.

References

[1] M. Zhang, S. Fang, A.A. Zakhidov, S.B. Lee, A.E. Aliev, C.D. Williams, K.R. Atkinson, R.H. Baughman, Science 309 (2005) 1215—1219.
[2] C. Dekker, S.J. Tans, M.H. Devoret, H. Dai, R.E. Smalley, A. Thess, L.J. Georliga, Nature 6624 (1997) 474—477.
[3] J. Lee, T. Jeong, J. Heo, S.-H. Park, D. Lee, J.-B. Park, H. Han, Y. Kwon, I. Kovalev, S.M. Yoon, Carbon 44 (2006) 2984.
[4] K.J. Ziegler, Z. Gu, H. Peng, E.L. Flor, R.H. Hauge, R.E. Smalley, J. Am. Chem. Soc. 127 (2005) 1541—1547.
[5] J. Liu, A.G. Rinzler, H. Dai, J.H. Hafner, R.K. Bradley, P.J. Boul, A. Lu, T. Iverson, K. Shelimov, C.B. Huffman, Science 280 (1998) 1253—1256.
[6] X.X. Wang, J.N. Wang, Carbon 46 (2008) 117—125.
[7] S. Wang, R. Liang, B. Wang, C. Zhang, Carbon 47 (2009) 53—57.
[8] J.N. Coleman, U. Khan, Y.K. Gun'ko, Adv. Mater. 18 (2006) 689—706.
[9] R. Xu, Z. Tan, D. Xiong, G. Fan, Q. Guo, J. Zhang, Y. Su, Z. Li, D. Zhang, Compos. Appl. Sci. Manuf. 96 (2017) 57—66.
[10] T. He, X. He, P. Tang, D. Chu, X. Wang, P. Li, Mater. Des. 114 (2017) 373—382.
[11] M. Prato, K. Kostarelos, A. Bianco, Acc. Chem. Res. 41 (2007) 60.
[12] C.H. Villa, M.R. McDevitt, F.E. Escorcia, D.A. Rey, M. Bergkvist, C.A. Batt, D.A. Scheinberg, Nano Lett. 8 (2008) 4221.
[13] M.R. McDevitt, D. Chattopadhyay, B.J. Kappel, J.S. Jaggi, S.R. Schiffman, C. Antczak, J.T. Njardarson, R. Brentjens, D.A. Scheinberg, J. Nucl. Med. 48 (2007) 1180—1189.
[14] H. Gao, Y. Kong, D. Cui, C.S. Ozkan, Nano Lett. 3 (2003) 471—473.
[15] A.L. Falk, K.-C. Chiu, D.B. Farmer, Q. Cao, J. Tersoff, Y.-H. Lee, P. Avouris, S.-J. Han, Phys. Rev. Lett. 118 (2017) 257401—257407.
[16] Q. Cao, J. Tersoff, D.B. Farmer, Y. Zhu, S.-J. Han, Science 356 (2017) 1369—1372.
[17] Z. Chen, K.J. Ziegler, J. Shaver, R.H. Hauge, R.E. Smalley, J. Phys. Chem. B 110 (2006) 11624—11627, 110.
[18] Z. Gu, H. Peng, R.H. Hauge, R.E. Smalley, J.L. Margrave, Nano Lett. 2 (2002) 1009—1013.
[19] N. Pierard, A. Fonseca, Z. Konya, I. Willems, G. Van Tendeloo, J.B. Nagy, Chem. Phys. Lett. 335 (2001) 1—8.
[20] N. Pierard, A. Fonseca, J.F. Colomer, C. Bossuot, J.M. Benoit, G. Van Tendeloo, J.P. Pirard, J.B. Nagy, Carbon 42 (2004) 1691—1697.
[21] J. Chen, M.J. Dyer, M.-F. Yu, J. Am. Chem. Soc. 123 (2001) 6201—6202.
[22] I. Stepanek, G. Maurin, P. Bernier, J. Gavillet, A. Loiseau, R. Edwards, O. Jaschinski, Chem. Phys. Lett. 331 (2000) 125.
[23] F. Banhart, J. Li, M. Terrones, Small 1 (2005) 953.
[24] S. Wang, Z. Liang, B. Wang, C. Zhang, Z. Rahman, Nanotechnology 18 (2007), 055301.
[25] S.R. Lustig, E.D. Boyes, R.H. French, T.D. Gierke, M.A. Harmer, P.B. Hietpas, A. Jagota, R.S. McLean, G.P. Mitchell, G.B. Onoa, Nano Lett. 3 (2003) 1007—1012.
[26] J. Xie, M.N. Ahmad, H. Bai, H. Li, W. Yang, Sci. China Chem. 53 (2010) 2026—2032.
[27] F. Ren, S.A. Kanaan, F. Khalkhal, C.Z. Loebick, G.L. Haller, L.D. Pfefferle, Carbon 63 (2013) 61—70.
[28] K. Mustonen, P. Laiho, A. Kaskela, Z. Zhu, O. Reynaud, N. Houbenov, Y. Tian, T. Susi, H. Jiang, A.G. Nasibulin, Appl. Phys. Lett. 107 (2015) 013106—013109.
[29] P. Laiho, K.A. Mustonen, Y. Ohno, S. Maruyama, E.I. Kauppinen, ACS Appl. Mater. Interfaces 9 (2017) 20738—20747.
[30] A. Moisala, A.G. Nasibulin, S.D. Shandakov, H. Jiang, E.I. Kauppinen, Carbon 43 (2005) 2066—2074.
[31] Y. Tian, M.Y. Timmermans, S. Kivistö, A.G. Nasibulin, Z. Zhu, H. Jiang, O.G. Okhotnikov, E.I. Kauppinen, Nano. Res. 4 (2011) 807—815.
[32] M.S. Dresselhaus, G. Dresselhaus, R. Saito, A. Jorio, Phys. Rep. 409 (2005) 47—99.
[33] Y. Tian, A.G. Nasibulin, B. Aitchison, T. Nikitin, J. v. Pfaler, H. Jiang, Z. Zhu, L. Khriachtchev, D.P. Brown, E.I. Kauppinen, J. Phys. Chem. C 115 (2011) 7309—7318.
[35] Y. Liao, H. Jiang, N. Wei, P. Laiho, Q. Zhang, S.A. Khan, E.I. Kauppinen, J. Am. Chem. Soc. 140 (2018) 9797—9800.